Twenty-Sixth Symposium (International) on Combustion/The Combustion Institute, 1996/pp. 1345–1352

EFFECTS OF SLOW WIND ON LOCALIZED RADIATIVE IGNITION AND TRANSITION TO FLAME SPREAD IN MICROGRAVITY*

T. KASHIWAGI AND K. B. McGRATTAN
National Institute of Standards and Technology
Gaithersburg, MD 20899, USA

S. L. OLSON
NASA Lewis Research Center
Cleveland, OH 44135, USA

O. FUJITA, M. KIKUCHI AND K. ITO
Hokkaido University
Sapporo, Japan

An experimental and numerical investigation of ignition and the subsequent transition to flame spread over a thermally thin cellulosic sample is described. The experiments were conducted using a lamp as an external radiant source in a 50% oxygen atmosphere at three different wind velocities of 0, 2, and 5 cm/s in a 10 s drop tower. The results show that there are no significant effects of the slow wind on the ignition-delay time. Photographic sequences of both the experiments and the calculations show that the wind increases the flame propagation speed in the upwind direction, while decreasing it in the downstream direction. The downstream flame fails the transition to flame spread and becomes a tail of the upstream flame. The downstream char front propagates much slower than that for the upstream direction. Three-dimensional, time-dependent numerical solutions to the Navier–Stokes equations are used to simulate the experiments. Three global degradation reactions describe the pyrolysis of the sample paper, and one gas-phase reaction describes the combustion of the fuel gases. The model results reflect the qualitative features of the experiments and also are in reasonable quantitative agreement, given the uncertainty of the gas-phase reaction mechanism.

Introduction

Although fire safety is absolutely essential in a human-occupied spacecraft, a few accidental incidents may be unavoidable, even with many precautions as to material selection and safety design. A momentary ignition followed by rapid extinction could be tolerable, but if the transition from ignition to flame spread occurs, crew safety could be jeopardized.

Although the fundamental processes involved in ignition and flame spread have been studied extensively [1–6], they were examined separately without combining ignition and flame spread through the transition process. A majority of experimental and theoretical studies conducted in microgravity were mainly steady state and two dimensional, and the transient aspects of ignition and the transition to flame spread were not studied in detail. Studies of more realistic configurations, such as localized ignition in the presence of a slow wind simulating ventilation in a spacecraft, are needed. In this case, a complex coupling exists between the flame fronts and the flow field that is manifested by such phenomena as the oxygen shadow observed when ignition occurs in the middle of a sample in a two-dimensional configuration [7]. In this paper, experiments and numerical calculations on localized radiative ignition of a thermally thin cellulosic filter paper in the presence of an external wind are analyzed with a focus on the transitional effects in the three-dimensional configuration.

Experimental Description and Results

A series of experiments was conducted in the 10 s drop tower at the Japan Microgravity Center (JAMIC). Only the results in 50% oxygen concentration are described in detail here because the available 10 s test time was sufficiently long to observe ignition and subsequent transition processes. A small

*Contribution from the National Institute of Standards and Technology; not subject to copyright.

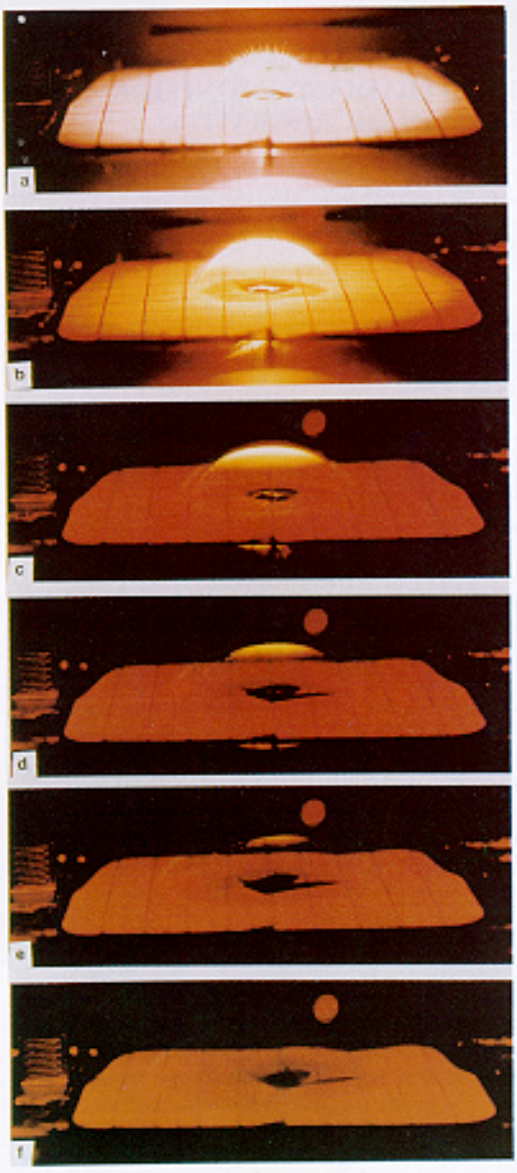

FIG. 1. Six photographs showing ignition and flame spread with no external wind. The frames are equally spaced, roughly 0.8 s apart, from the time of ignition. The grid lines are spaced 1 cm apart.

fan was used to generate a slow uniform external flow velocity up to 5 cm/s. The test section was 85 mm wide × 95 mm high × 171 mm long, and the test chamber was installed in a large enclosed chamber (about 90 l volume used as a reservoir).

A small tungsten/halogen lamp was used as an ignitor. The lamp power was turned on at the start of a drop, and the power to the lamp was measured during each test. The lamp was turned off at a specified time after ignition was achieved. The emission spectra of the lamp were measured from 2 to 20 μm using a FTIR, and its transient radiant flux at the sample surface was measured (it took about 1 s for its emission flux to start to increase and additional 1.2 s to reach a peak flux of 10 kW/m^2 and its distribution was Gaussian with a half width of about 0.5 cm.). A 10 × 8.7 cm sheet of Whatman ashless filter 44 was used as the sample paper.* The center part of the sheet over the irradiated area was blackened to increase absorption of the incident beam from the lamp. The absorptivity of the blackened paper was measured by the NIST radiometric group from 1 to 20 μm. Color video pictures were taken in the direction normal to the sample surface to observe ignition and changes in the flame shape and char pattern. Red diodes were used to illuminate the sample surface. Still color photographs were taken at an oblique angle to the sample by a motor-driven 35-mm camera.

Ignition of the sample paper coincided with a popping sound recorded on videotape. Ignition-delay times were 3.6, 3.6, and 3.7 s for the 0-, 2-, and 5-cm/s cases, respectively. No significant effects of the wind on ignition time were observed for the range of wind velocities used in this study. Photographic sequences of the ignition, transition, and flame spread are shown in Figs. 1–3. Since a blue color window was not used for Figs. 1 and 3, the color of the paper sample appears to be red, reflecting the red diode backlight. The first frame of Fig. 1 shows a hemispherical flame shortly after ignition. Note the small spikes on the flame surface at ignition. It is speculated that this is caused by the ejection of soot particles during the sudden expansion of the gas. Shortly after ignition, the lamp is turned off and the supply of degradation products is gradually decreased. The orange part of the flame gradually disappears, and the periphery of the flame starts to spread outward. The flame front is faint blue, and it is difficult to see in Fig. 1.

In Fig. 2, a blue window was used and blue flame front and charred surface can be seen better than the other two cases. The shape of the flame shortly after ignition is nearly hemispherical with a slight slant downstream due to the 2-cm/s wind. The periphery of the flame starts to spread outward and the faint blue flame front is seen in the upstream portion of the flame in Fig. 2c. The orange color of the upper portion of the flame gradually fades out and no orange color is seen in Fig. 2f. A blue flame front is

*Certain company products are mentioned in the text to specify adequately the experimental procedure and equipment used. In no cases does such identification imply recommendation or endorsement by the National Institute of Standards and Technology, nor does it imply that the products are necessarily the best available for the purpose.

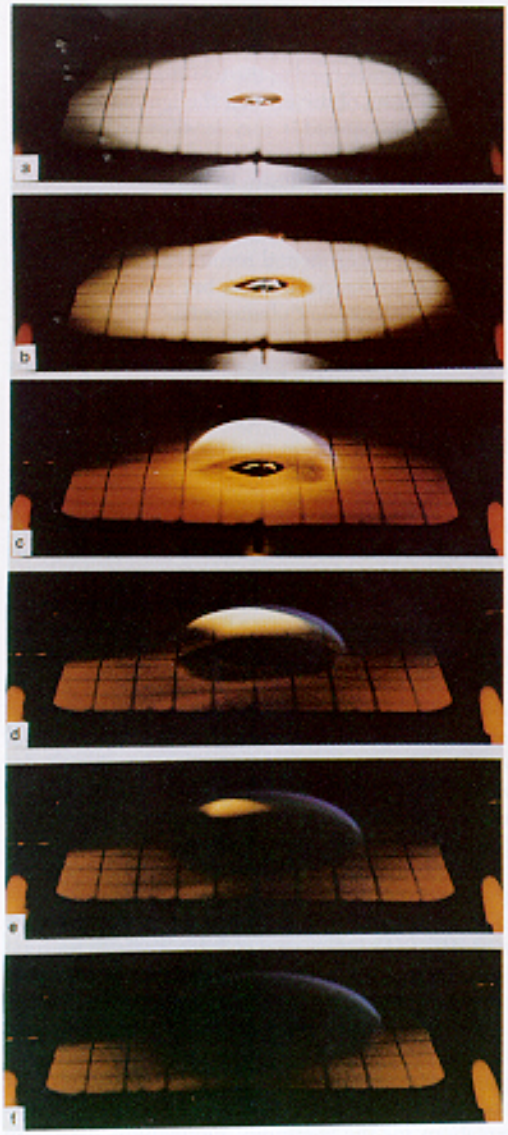

FIG. 2. Six photographs showing ignition and flame spread with a 2-cm/s external wind blowing from right to left. The frames are equally spaced, roughly 0.8 s apart, from the time of ignition.

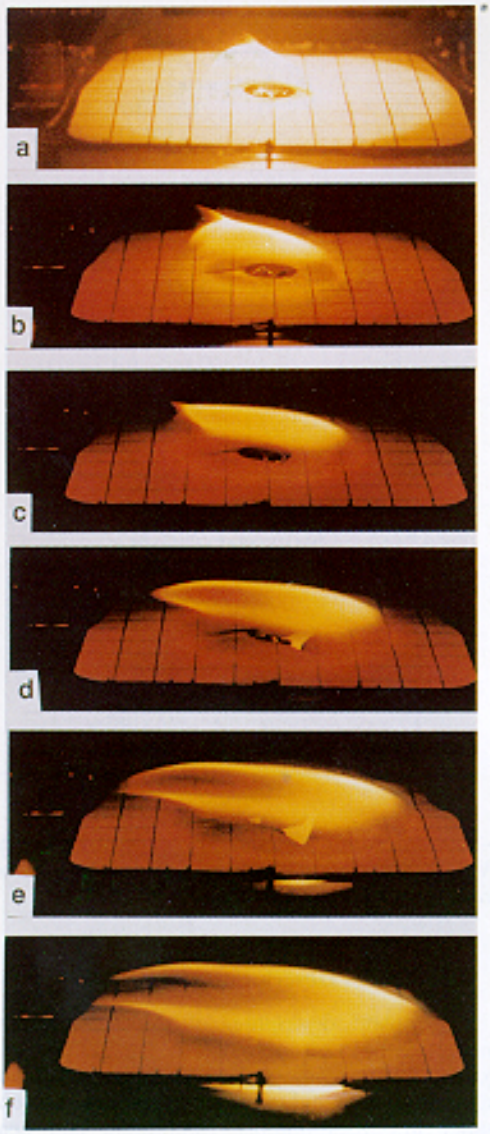

FIG. 3. Six photographs showing ignition and flame spread with a 5-cm/s external wind blowing from right to left. The frames are equally spaced, roughly 0.8 s apart, from the time of ignition.

not observed on the downstream side and char growth is faster in the upstream direction.

In the case of a 5-cm/s wind (Fig. 3), the flame is more elongated in the downstream direction and its color is much more orange than the other two cases. The most interesting feature of this flame is its horseshoe shape and the absence of flame along the centerline downstream of the ignition point. The upstream portion of the flame is close to the sample surface, and it gradually lifts off from the surface further downstream.

Because the flame fronts in all three cases are difficult to distinguish clearly, the char pattern left behind was used to measure spread rates. The growth pattern of the char front shows a similar trend with that of the flame front. The upstream char front spread rates for the 2- and 5-cm/s winds are 0.48 and 0.76 cm/s, respectively. The sidewise char front spread rates (normal to the flow direction) for 2- and

TABLE 1

Pyrolysis reaction	
A_p	3.0×10^{18} min^{-1}
E_p	237 kJ/mol
n_p	1.2
$\nu_{char,p}$	0.14
$\nu_{sf,p}$	0.23
ΔH_p	64 J/g
Oxidative degradation reaction	
A_{ox}	5.0×10^{18} min^{-1}
E_{ox}	224 kJ/mol
n_{ox}	0.4
$n_{j,ox}$	1.0
$\nu_{char,ox}$	0.2
$\nu_{sf,px}$	0.16
$\nu_{O_2,ox}$	0.41
ΔH_{ox}	1000 J/g
Char oxidation reaction	
A_{char}	1.0×10^{11} min^{-1}
E_{char}	166 kJ/mol
n_{char}	1.0
$n_{O_2,char}$	1.0
$\nu_{ash,char}$	0.02
$\nu_{sf,char}$	0.52
$\nu_{O_2,char}$	1.65
ΔH_{char}	2400 J/g

5-cm/s winds are 0.43 and 0.66 cm/s, respectively. Without any wind, it is 0.36 cm/s, the average of the front speeds in four directions.

Model Description and Results

A complete description of the mathematical model has been given in Ref. 7. The gas phase is governed by the conservation equations of mass, momentum, energy, and species (fuel gases and oxygen) under low-Mach-number combustion and heat transfer conditions. In past work (two-dimensional configuration), it was assumed that the velocity field was approximated by a potential flow [7]. Now, the full Navier–Stokes form of the momentum conservation equation (in three-dimensional configuration) is solved. However, the potential flow approximation is used to apply boundary conditions since the rapid expansion at ignition cannot be treated properly with conventional zero-gradient boundary conditions. The uniform inlet flow condition is specified at the upstream edge of a paper sample and a boundary layer along the sample surface is calculated. The gas-phase oxidation reaction is represented by a global one-step reaction characterized by a second-order Arrhenius rate equation. The preexponential factor is 5.0×10^9 cm^3/(g·s), and the activation energy is 67 kJ/mol. The heat of combustion is 35 kJ/g, and the stoichiometric constant is 3.57. These values are the same as those used in the two-dimensional study [7]. It has been observed that the ignition and transition to flame spread is very sensitive to the choice of the gas-phase reaction constants. The present choice is guided by a desire to match roughly flame spread rates with the experiments of Olson [3]. However, the objective of the study is not necessarily to duplicate experimental results exactly by manipulating the model parameters but rather to deduce trends of the transient phenomena.

The sample used in the experiments is more thermally stable than the paper used in our previous study [7,9]. Its thickness is 0.13 mm, area density 5.7 mg/cm^2, and specific heat 0.96 J/(g·K). It is assumed that this value of specific heat applies to the char and ash, as well, and increases linearly with temperature [8]. It is assumed that the sheet is thermally thin and also of uniform composition through its depth. Radiative loss from the sample surface is included but radiation from the flame is not included in the model, and the emissivity of the sample is estimated to be 0.6 [8]. The measured lamp radiative heat flux distribution at the sample surface is used and the reflectivity is calculated to be 0.25 from the emission spectra of the lamp and the measured hemispherical surface reflectance as described in the Experimental section. The pyrolysis of the cellulosic sheet is described by a slightly exothermic global pyrolysis reaction, an exothermic global thermal oxidative degradation reaction, and an exothermic global char oxidation reaction. The kinetic constants for each degradation reaction were derived with the same type of thermogravimetric analysis used in our previous study [9] and summarized in Table 1. Yields for total hydrocarbons, CO, CO_2, H_2O, and the consumption of oxygen were taken from previous studies.

The three solid-phase degradation reactions are written as a system of conservation equations for mass, cellulose, char, and energy and solved using an ordinary differential equation stiff solver [7]. The equations for the continuity, momentum, gas-phase temperature, and two species concentrations are written in finite difference form and solved with a simple time splitting scheme in which it is assumed that the oxidative reaction occurs over a small part of the overall time step and the convective and diffusive terms are differenced and updated with an ADI (alternating direction implicit) scheme. The momentum equation is solved with a simple projection method that relies on the prescription of the velocity field at the boundary of the computational domain. This boundary velocity is provided by the potential flow approximation. A Poisson equation for pressure is solved with a direct solver. Cells in the three-dimensional grid are typically about 1 mm in the directions parallel to the sample surface. Cells in the normal direction are about 0.25 mm at the

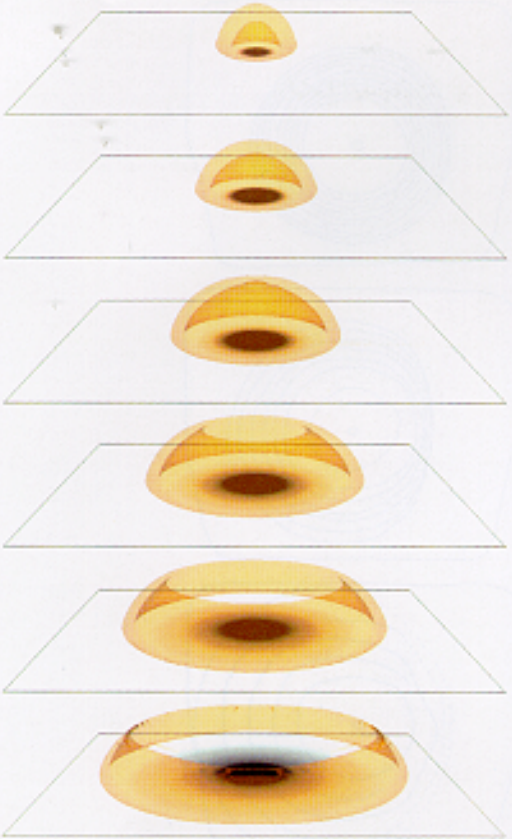

FIG. 4. Six views of the numerically simulated flame with no external wind. A three-dimensional surface with a constant of gas-phase reaction rate, 10^{-4} g/cm^3 s, is shown. (The darker region is due to overlapping of the surfaces.) The resulting char pattern can be seen through the surface. The time sequences are approximately the same as those in Fig. 1.

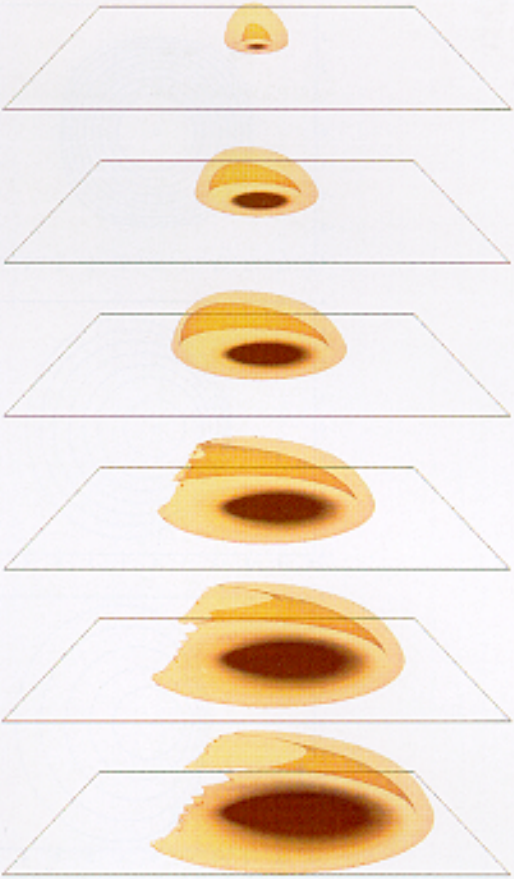

FIG. 5. Six views of the numerically simulated flame with a 5-cm/s wind blowing from right to left. A three-dimensional surface with a contour of constant gas-phase reaction rate, 10^{-4} g/cm^3 s, is shown (the darker region is due to overlapping of the surfaces). The resulting char pattern can be seen through the surface. The time sequences are approximately the same as those in Fig. 3.

sample surface and expand to about 2 mm farther from the surface. For the simulations described later, the computational domain was 10 cm in the windward direction, 5 cm spanning half of the lateral direction, and 5 cm in the normal direction. Symmetry is assumed about the plane that is spanned by vectors normal to the paper surface and parallel to the wind direction. Also, the paper itself is assumed to be a plane of symmetry. A typical grid contains about 260,000 cells ($128 \times 64 \times 32$), and the calculations require about 48 h CPU time on a current generation workstation for 5 s simulation of the events.

Three experiments were chosen to compare with numerical simulations. Each of the selected experiments involved the spot ignition of the paper in an atmosphere of 50% oxygen with imposed winds of 0, 2, and 5 cm/s. Figure 4 displays the results of the 0 cm/s computation. Shown is a sequence of snapshots that depict the evolution of the visible flame from ignition through the transition to flame spread. The ignition is achieved at about 2.6 s and there are no significant effects of wind on ignition-delay time. The flame initially takes the shape of a hemispherical dome, which eventually opens up as the flame propagates in the outward direction. The char pattern is also shown on the paper surface. It expands outward 3–4 mm behind the flame front. The effects of 5-cm/s wind on ignition and the transition to flame spread are shown in Fig. 5. The initial shape of the flame is similar to the previous case since the flow field is dominated by the rapid thermal expansion. However, after ignition, the wind be-

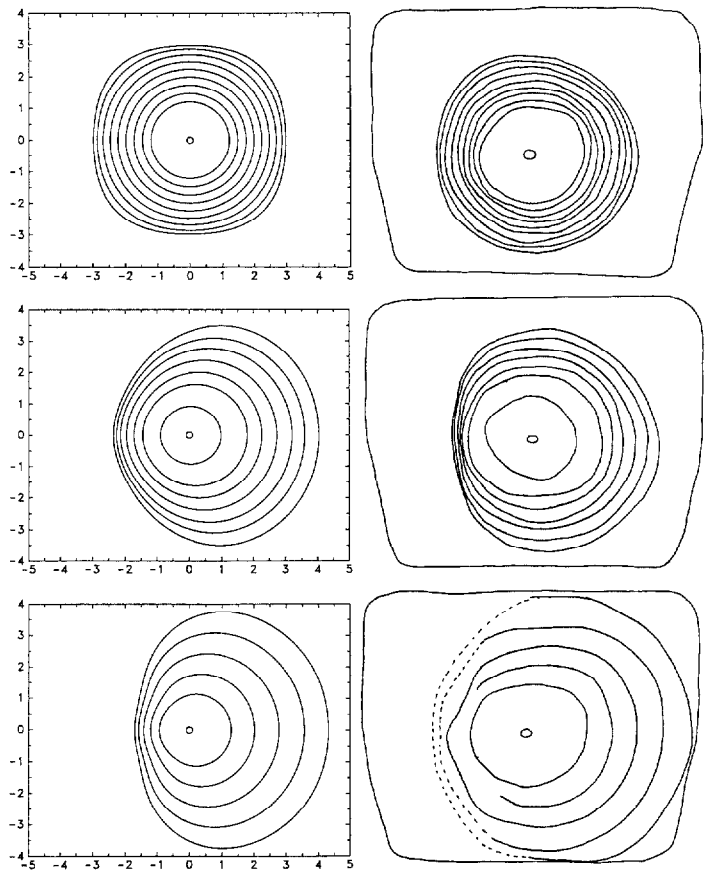

FIG. 6. Numerical (left) and experimental (right) char front histories for winds of 0, 2, and 5 cm/s blowing from right to left. The numerical fronts were plotted at times equivalent to the those of the experiment (from the ignition time). The fronts for the no wind case are separated by 0.5 s, for the 2 cm/s case 0.67 s, and for the 5 cm/s case 1.0 s. The dimensions of the experimental sample sheets are comparable to those of the calculations.

gins to reshape the flame front into a horseshoe pointed into the wind. In the fourth picture, the tail end of the downstream flame begins to disappear and this process continues in the next two frames. Both the upstream flame front and upstream char front rapidly spread toward the incoming flow. The standoff distance of the upstream flame front is less than 1 mm, but this distance gradually increases towards the lateral tips of the flame where the standoff distance is several millimeters.

The char front patterns shown in Fig. 6 (left-hand side) are for the same times as those of the actual experiments, shown in the right-hand side in the same figure. In the calculation, the char front is defined when the normalized density of the sample becomes 0.9. From the char front histories, the upstream char front in the windblown cases propagated at speeds of 0.46, 0.62, and 0.76 cm/s for the 0, 2, and 5 cm/s imposed wind. These results and the three char patterns show clearly that the wind increases upstream char front propagation but it slows the downstream char front propagation.

Discussion

The predicted ignition-delay time of 2.6 s is shorter than the 3.6 s ± 0.1 observed in the experiment, but both the experiments and the calculations indicate no significant effects of wind on ignition-delay time. The difference in delay time is due mainly to uncertainties in the reflectivity, emissivity, and specific heat of the sample. The char and flame front patterns of both the experiment and the numerical model are in good agreement. Both the experiments and the model show that the upstream flame and char front spread rates increase with increased wind velocity. The calculated char front spread rates are 0.46, 0.62, and 0.76 cm/s for 0, 2, and 5 cm/s, respectively, compared to the measured

values of 0.36 ± 0.06, 0.48 ± 0.04, and 0.76 ± 0.03 cm/s, respectively. There are no significant differences in the experimental/theoretical upward char front spread rates between the three-dimensional configuration and the two-dimensional configuration.

The calculated sidewise char front spread rates (normal to the flow direction) are 0.45 and 0.50 cm/s for 2 and 5 cm/s compared to the measured rates of 0.43 ± 0.05 and 0.66 ± 0.02, respectively. With wind, both show that the downstream flame front lifts off from the sample surface during the transition period and becomes the extended tail of the upstream flame. For a 5-cm/s wind, both model and experimental flames take on a characteristic horseshoe shape, while the char pattern takes on an oval shape biased in the upwind direction. Since the standoff distance between the flame and the sample surface is much larger in the downstream flame than in the upstream flame, it is expected that the heat feedback rate from the flame to the surface is much less for the downstream flame than for the upstream flame. The gas phase reaction zone shown in Fig. 5 is fueled by a horseshoe-shaped area of the sample surface where the heat flux from the flame was calculated to be greater than 2 W/cm^2. The peak flux is about 4.5 W/cm^2 at the upstream flame front. The center of the downstream front shows a heat feedback of 1.6 W/cm^2. Between the fronts, the flux is roughly 1 W/cm^2.

The calculated oxygen concentration near the sample surface shows that there is hardly any oxygen left within the region encircled by the flame, and neither convective nor diffusive transport is sufficient to replenish it. This depleted oxygen region extends far downwind past the charred area in the cases of an imposed wind. The upstream bias of the windblown flames is due to the convective resupply of oxygen to the upwind front and the subsequent oxygen shadow experienced by the downstream front. The rapid expansion of the heated gases generates a dome-shaped structure around which the fresh air is forced to flow, depriving the downstream flame of oxygen.

Conclusions

The experiments have shown that the ignition of a paper sample by radiative heating is accompanied by a noticeable pop and a spiked flame shape caused by a dramatic burst of degradation products. There are no significant effects of a slow wind on the ignition-delay time for the range of velocities used in the experiments. Wind effects become important, however, during and after the transition from ignition to flame spread is achieved. Then the upstream flame front spreads most rapidly, followed by the lateral fronts. The downstream flame fails the transition to flame spread and becomes the tail of the upstream flame. Thus, degradation of the paper sample is halted a few centimeters downwind of the ignition point, as evidenced by the resulting char pattern.

The three-dimensional, time-dependent numerical model captures these features quite well with carefully measured solid-phase kinetic constants, but the gas-phase kinetics are more uncertain. These parameters need to be chosen to produce results in rough agreement with observed phenomena.

Acknowledgments

This study is supported by the NASA Microgravity Science Program under the Inter-Agency Agreement No. C-32001-R. The JAMIC experiments were funded by NASA and the New Energy and Industrial Technology Development Organization (NEDO) through the Japan Space Utilization Promotion Center.

REFERENCES

1. de Ris, J. N., *Twelfth Symposium (International) on Combustion,* The Combustion Institute, Pittsburgh, 1969, pp. 241–252.
2. Olson, S. L., Ferkul, P. V., and Tien, J. S., *Twenty-Second Symposium (International) on Combustion,* The Combustion Institute, Pittsburgh, 1988, pp. 1213–1222.
3. Olson, S. L., *Combust. Sci. Technol.* 76:233–249 (1991).
4. Bhattacharjee, S., Altenkirch, R. A., and Sacksteder, K. R., *Combust. Sci. Technol.* 91:225–242 (1991).
5. Ferkul, P. V. and Tien, J. S., *Combust. Sci. Technol.* 99:345–370 (1993).
6. di Blasi, C., *Combust. Flame* 100:332–340 (1995).
7. McGrattan, K. B., Kashiwagi, T., Baum, H. R., and Olson, S. L., "Effects of Ignition and Wind on the Transition to Flame Spread in a Microgravity Environment," *Combust. Flame* 106:369–391 (1996).
8. Milosavljevic, I., "Behavior of Charring Materials in Simulated Fire Environments," Ph.D. Thesis, Division of Engineering, Brown University, January 1994.
9. Kashiwagi, T. and Nambu, H., *Combust. Flame* 88:345–368 (1992).

COMMENTS

M. A. Delichatsios, FMRC, USA. The authors should compare their results with simple energy balance methods to obtain key creeping flame spread properties. In this way they could extend the prediction of flame spread rates for other imposed wind speeds without performing lengthy numerical calculations.

Author's Reply. First, we are studying ignition and the transition to flame spread thus our interests are not limited to steady flame spread phenomena. A simple energy balance approach suggested is useful, but generally it tends to be limited by the empirical information used and approximations/assumptions which are not rigorously validated. It might be useful to derive and examine the validity of such a simple model after rigorous examination of the detailed calculated and experimental results (not only flame spread rate but temperature distribution, flow field, heat feedback rate, and other important characteristics).

•

Subrata Bhattacharjee, San Diego State University, USA. Could you comment on how steady the post-ignition spread was in the case of quiescent environment? Also, a comparison of spread rates and flame shapes between the symmetric spread, and that over samples of finite width [1] may validate the widely-used assumption of two-dimensionality in flame spread modeling.

REFERENCE

1. Bhattacharjee, S. and Altenkirch, R. A., *Twenty-Fourth Symposium (International) on Combustion,* The Combustion Institute, Pittsburgh, 1992, pp. 1669–1676.

Author's Reply. In a quiescent 50% oxygen atmosphere used in this study, the flame spread rate away from the irradiated area is basically steady for both two- and three-dimensional configurations. As shown in the figures in the paper, initially an orange color flame is seen in the center with a blue flame front at the perimeter. With increasing time, the central orange flame becomes faint and eventually it disappears, and only the faint blue flame remains. It appears that the central orange flame does not have significant effects on flame spread rate. The averaged flame spread rate in a quiescent 50% oxygen atmosphere is 0.36 $\pm$ .06 cm/s which agrees well with the data measured by Professor Bhattacharjee and his colleagues. However, since our filter paper (Whatman 44) is different from their filter paper (if I understand correctly, their paper was Whatman 1 and it appears that our paper is slightly thinner than theirs), it might need some caution to compare the experimental results directly. It is important to confirm the two-dimensionality as pointed out by Professor Bhattacharjee. In the slow flow regime in microgravity, the flow field clearly has an elliptic nature, and a narrow sample or a small enclosure might cause three-dimensional effects.